Sustainable Energy & Fuels

ROYAL SOCIETY OF CHEMISTRY

PAPER

View Article Online
View Journal | View Issue

Cite this: *Sustainable Energy Fuels*, 2025, **9**, 3693

Received 6th February 2025
Accepted 4th May 2025

DOI: 10.1039/d5se00181a

rsc.li/sustainable-energy

Stable lithium plating/stripping electrochemistry promoted by a MnO_2 modified copper current collector for stable lithium metal anodes†

Bidhan Pandit *[a] and Chun Huang*[abc]

Due to lower redox potential and excellent theoretical capacity, lithium metal anodes are being explored for high-energy density next generation rechargeable batteries. The lithium metal anode is dragged out of use in practical applications because of its high reactivity and considerable volume expansion, which also cause an unstable solid electrolyte interface, severe side reactions, dendrite growth, electrode degradation, low coulombic efficiency, and even significant safety concerns. To establish a stable solid electrolyte interphase (SEI) and avoid dendrite issues, a variety of methods are being investigated. It is also shown that the initial Li nucleation, which determines the interface and reversibility of future cycles, may be aided by the deposition of a thin film of MnO_2 on the current collector. By lowering the electrode's nucleation barrier, the lithiophilic properties of MnO_2 may successfully promote smooth and homogeneous plating of Li on the Cu collector surface. Such a MnO_2 nanorod structure enables effective electron conduction between the conductive substrate and lithiophilic layer, improves Li-ion

[a]*Department of Materials, Imperial College London, South Kensington Campus, Exhibition Road, London SW7 2AZ, UK. E-mail: physics.bidhan@gmail.com; b.pandit@imperial.ac.uk; a.huang@imperial.ac.uk*

[b]*The Faraday Institution, Quad One, Becquerel Ave, Harwell Campus, Didcot, OX11 0RA, UK*

[c]*Research Complex at Harwell, Rutherford Appleton Laboratory, Didcot, OX11 0FA, UK*

† Electronic supplementary information (ESI) available. See DOI: https://doi.org/10.1039/d5se00181a

Bidhan Pandit

Bidhan Pandit is now a Marie Curie Energy for Future (E4F) Fellow at Imperial College London, United Kingdom. He received his PhD in Physics from Visvesvaraya National Institute of Technology, India, in 2019. Following his doctoral studies, he undertook a CNRS Postdoctoral Research Fellowship at the Institut Charles Gerhardt Montpellier (ICGM), Université de Montpellier, France (2019–2021). Subsequently, he was appointed as an Assistant Professor and Marie Curie CONEX-Plus Fellow at Universidad Carlos III de Madrid (UC3M), Spain (2021–2024). His previous scientific interests focus on the synthesis of nanostructures and fabrication of flexible devices for supercapacitor applications. His current research focus includes the synthesis of cathode materials for lithium, sodium and potassium-ion batteries, as well as the in situ/operando X-ray based characterization techniques for the understanding of battery mechanisms.

Chun Huang

Chun Huang is currently a Reader in Energy Storage Materials at the Department of Materials, Imperial College London. She completed her Bachelor's degree in Materials Science and Engineering (First Class Honours) at Imperial College London and PhD degree in Materials Science at the University of Oxford. She worked as a Lecturer at King's College London before moving to Imperial College London. Her research focuses on new materials for lithium ion batteries, sodium ion batteries, and solid-state batteries, and operando X-ray characterisation techniques. She has been awarded the European Research Council (ERC) Starting Grant and the UKRI EPSRC Innovation Fellowship.

transfer kinetics, and significantly minimizes the local current inhomogeneity. The structure effectively prevents dendritic growth and volume change as evidenced by its ability to retain a constant coulombic efficiency over an extended period of time of up to 186 h (2 mA cm^{-2}). This technology has made it possible to demonstrate Li metal anodes with excellent coulombic efficiency, paving the way for steady, efficient, and long-cycle life Li metal batteries with less Li loading.

1. Introduction

The progress of inexpensive and sustainable energy storage technology is crucial given the world's insatiable desire for energy.[1–3] Due to their performance in terms of safety during cyclic charge/discharge operations with intercalation reactions, lithium-ion batteries (LIBs) are now extensively employed in numerous applications, including portable devices, electric vehicles (EVs), and smart grids.[4–7] However, consumers' current preference for and pursuit of mobility causes additional issues for LIBs with regard to high energy density demand.[8–10] Due to its very low redox potential of −3.04 V *versus* SHE and high theoretical capacity (2061 mA h cm^{-3} and 3860 mA h g^{-1}, respectively), lithium metal is the perfect choice as an anode for rechargeable batteries.[11–14] The usage of lithium metal anodes in rechargeable batteries, such as Li metal batteries,[15–17] Li–S batteries,[18–20] and Li–air batteries[21–23] has lately gained a lot of attention due to the urgent requirement for high energy density batteries.

Li forms dendritic growth because inhomogeneous nuclei are produced by non-uniform current and Li^+ flux.[24,25] The absence of a host is what causes the morphology of the nucleus to be unstable. Li dendrites are more likely to penetrate through the separator when dendritic Li develops, resulting in battery short circuits, even explosion or combustion.[26–28] Additionally, due to the spontaneous interaction of Li metal with Li salt anions and electrolyte solvents, a solid electrolyte interphase (SEI) layer develops on the metallic Li surface.[29–31] The weak SEI will ultimately break down because of the frequent Li plating and stripping, which increases the exposure of Li metal to electrolyte and results in strong side reactions between electrolyte and Li in addition to poor coulombic efficiency (CE).[32] The anode's volume also goes through a totally new process that results in significant volume variations throughout charge/discharge processes.[33–35] Internal tension and the solid–liquid interface alter as a result of this transformation. Thermal runaway, internal short circuits, or even an explosion might ensue from the dendritic growth by heterogeneous Li deposition.[36–38] As a result, Li metal batteries (LMBs) have struggled extremely, which has resulted in low CE, rapid cycle durations, and even safety issues.[39,40] The SEI may continue to break and form as long as the deposition procedure is continuing. More dendritic Li is exposed to the electrolyte because of its increased surface area. It uses a lot of electrolytes as a result, in addition to working on the rapid development of Li dendrites and Li inventory. The use of lithium metal anode for commercial applications is limited by these issues.[41,42]

So far, lithium alloys,[43–45] electrolyte additives,[46–48] synthetic SEI films,[49–51] 3D Li hosts,[52–54] and solid/gel electrolytes[55–57] have all been used as ways to stop lithium dendrite growth and keep the electrode/electrolyte interface stable. However, the Li dendrite development is difficult to control well, and the additive will be consumed completely. The introduced protective layer may be damaged and peeled off from the electrode owing to the volumetric change during a cycle, and solid electrolytes have low ionic conductivity. It is thus recommended to choose an electrode with a broad surface area that is rich in channels and/or porosity in order to lessen volume expansion and scatter local current intensities for homogeneous Li deposition. Because of their ability to effectively block the dendrite due to the spatial impact, metal oxides with a range of structures, such as ZnO nanorod arrays,[58] Cu_2O nanoparticles,[59] CuO nanosheets,[60] Co_3O_4 nanoarrays[61] *etc.*, are gaining a lot of attention as modified current collectors.

In this study, a lithium metal anode is stabilized on MnO_2 nanorods that are deposited on a bare Cu current collector (MnO_2@Cu) when using 1 M lithium bis-(trifluoromethane) sulfonimide (LiTFSI) in dioxolane/dimethoxyethane (DOL/DME) (1 : 1, v/v) with a 2% addition of lithium nitrate ($LiNO_3$) additive as the electrolyte. The selection of 1 M LiTFSI in DOL/DME (1 : 1, v/v) with 2% $LiNO_3$ as the electrolyte is based on its well-documented efficacy in lithium–sulfur (Li–S) battery systems.[62,63] The nature of the solution plays a more crucial role in Li–S batteries than ordinary Li-ion batteries, since it not only acts as an ionic conductor for mass transfer but also participates substantially in the conversion processes of both lithium and sulfur. The DOL/DME solvent combination assists in balancing polysulfide solubility, decreasing the shuttle effect, and enhancing cycle life.[64,65] $LiNO_3$ facilitates the establishment of a stable SEI on the lithium metal anode, limiting dendrite growth and side reactions. LiTFSI enables strong ionic conductivity while limiting reactivity with lithium metal compared to other lithium salts.[66,67] This electrolyte solution allows steady long-term cycling, which is crucial for lithium–sulfur battery applications. The choice of electrolyte remains significant owing to its known compatibility with lithium metal anodes and its efficacy in tackling the primary difficulties of lithium–sulfur batteries. Moreover, the following benefits of the MnO_2@Cu host make it feasible to properly control the Li deposition properties: (i) a large-surface-area porous conductive structure that effectively reduces the local current density, (ii) a porous structure that accommodates quick volume expansion at high current, (iii) a stable skeleton that buffers compressive stress in the course of long cycling, (iv) lithiophilic sites that homogenizes Li deposition and direct the distribution of crystal nuclei, and (v) the reversible reactions to efficiently remove nucleation barriers. In fact, the uniformly distributed MnO_2 nanorods, after forming a stable SEI just after the plating step, increase the substrate's lithophilic properties, offer a significant number of lithium plating sites, direct homogeneous Li^+ flux

scattering, and speed up lithium transportation. This can control the following plating and stripping steps as well as dramatically decrease the nucleation barrier of lithium at a primary phase. As a consequence, MnO_2@Cu shows an average CE of 84% over 100 cycles at a current density of 2 mA cm^{-2} with a fixed capacity of 2 mA h cm^{-2}, greater than that of the cell with the Cu anode (35 cycles), demonstrating its encouraging potential for usage in real-world applications. Even at high areal capacity deposition, the compositional and structural advantages allow for a homogeneous and steady lithium plating on MnO_2@Cu. MnO_2@Cu performs as predicted, offering a high CE, dendrite-free lithium plating and stripping performance across 20 cycles at sequentially increasing current densities (2–5 mA cm^{-2}). At extremely high current densities greater than 5 mA cm^{-2}, MnO_2@Cu cells significantly outperform conventional cells regarding steady cycling and rate capability performance.

2. Experimental section

2.1. Synthesis of MnO_2

Manganese(II) acetate as a manganese precursor was oxidized with ammonium persulfate for MnO_2 preparation (Fig. 1), as per our previous report.[68] For the necessary synthesis, 100 mL of sodium hydroxide was first developed and separated into two beakers; one for the manganese and other for the ammonium persulfate precursor. Then, they were mixed and placed in a Teflon-coated autoclave. The arrangement was maintained at 180 °C for 14 h. The resulting product was cleaned in water and ethanol, followed by a drying process for 12 hours at 60 °C. The final product was annealed at 350 °C in an oven for 4 h.

Our method for preparing manganese dioxide involves two synthetic processes. The interaction between sodium hydroxide and the manganese precursor results in the formation of a manganese hydroxide compound:

$$(CH_3COO)_2Mn + 3OH^- \rightarrow Mn(OH)_3^- + 2CH_3COO^- \quad (1)$$

Taking into account the first step, the second one is associated with the reaction process involving persulfate anions and manganese hydroxide:

$$Mn(OH)_3^- + S_2O_8^{2-} + OH^- \rightarrow MnO_2 + 2SO_4^{2-} + 2H_2O \quad (2)$$

The details about materials characterizations are as per Note S1.†

2.2. Electrochemistry measurements

In order to prepare the electrodes, poly(vinylidene fluoride) (PVdF) was used as a binder in the solvent 1-methyl-2-pyrrolidinone (NMP).[69,70] A homogeneously mixed slurry comprising MnO_2 (88%) and binder (12%) was tape cast onto copper foil, dried at ambient temperature for 12 hours, and then dried under vacuum at 80 °C for one day.[71,72] The total area of the electrodes was 1.13 cm^2.

For the fabrication of 2032 coin-type cells with a Li metal sheet as reference and counter electrodes, electrochemical performance was analyzed. Half-cells were prepared by employing an electrolyte of 1 M LiTFSI in DOL/DME (1 : 1, v/v) with 2% $LiNO_3$ additive. Note that each cell's electrolyte content was kept constant at 160 µl. A glovebox containing high-quality argon with less than 1 ppm oxygen and water was used to construct all of the coin cells. Glass fiber from Whatman was used as a separator. Then, tests for electrochemical analysis were conducted at several capacities and current densities with a fixed 0.5 V cutoff voltage.

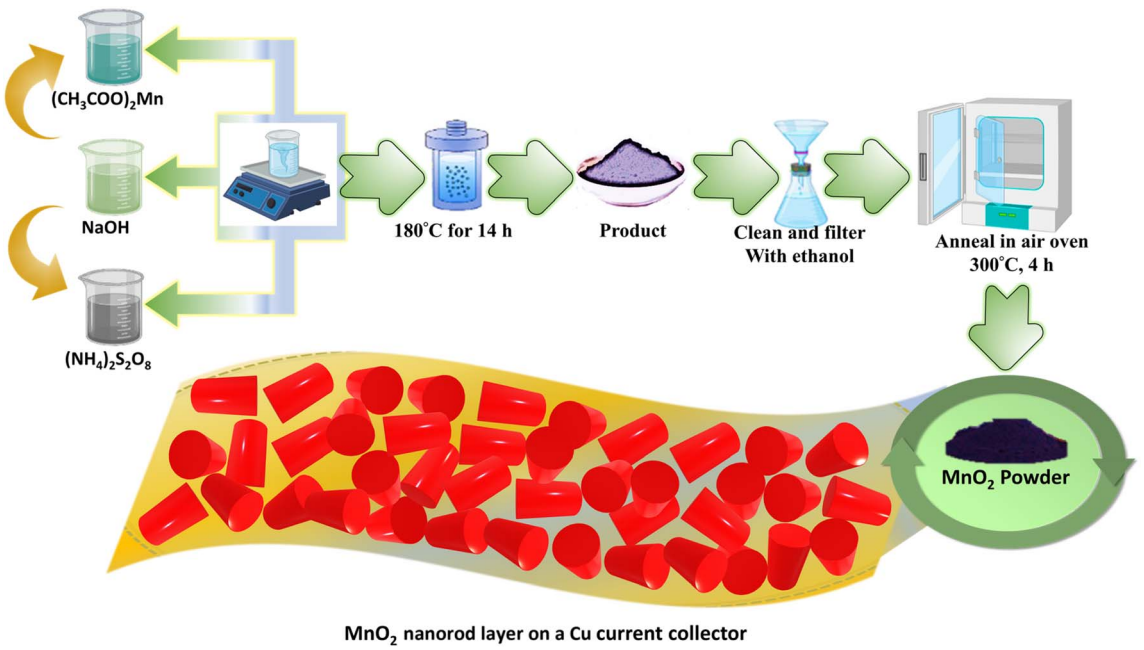

Fig. 1 Schematic illustration of MnO_2 synthesis.

3. Results and discussion

3.1. Structural and morphological analysis

Detailed structural and morphological analysis has been already reported in our previous article.[73] However, significant characterizations and discussions have been emphasised here. The important XRD pattern associated with Rietveld refinement is shown in Fig. S1a,† utilizing a pseudo-Voigt work function, confirming the tetragonal structure of MnO_2. Various crystallographic planes are identified by the distinct diffraction peaks. The profile coefficients and cross fragment cutoff were altered using the Rietveld method. The results show that the experimental pattern (dark circles) and selected model (red line) have a respectable agreement for the *I*4/*m* space group using our technique. The oxidation states of the synthesized material were examined using the XPS spectrum. The core-level standard XPS spectra of Mn 2p is displayed in Fig. S1b.† The Mn 2p spectrum is split into a doublet, with peaks at 642.5 and 654 eV and may be easily distinguished from $2p_{3/2}$ and $2p_{1/2}$, separately, according to Fig. S1b.† The manganese in MnO_2 is believed to be in the +4 oxidation state since the limiting energy difference between the aforementioned Mn 2p doublet is around 11.5 eV.[74]

The high-resolution transmission electron microscopy (HRTEM) image in Fig. S1c† demonstrates that the average diameter of as-prepared MnO_2 nanorods is in the range of 10–30 nm. The selected area electron diffraction (SAED) pattern of the structure in Fig. S1d† again demonstrates the diffraction spots that are clearly identifiable as originating from the crystallographic planes of the structure.

3.2. Electrochemical behavior of Cu and MnO_2@Cu current collectors

To investigate the electrochemical properties, the half cells of Li//Cu and Li//MnO_2@Cu were constructed. The half-cells were also cycled at 2 mA cm^{-2} and a constant plating/stripping capacity of 2 mA h/cm^2 for each cycle in order to understand how MnO_2 on Cu affects the cycle stability (Fig. 2 and 3). The Li//MnO_2@Cu battery offers more stable and long-term plating/stripping cycles than the Li//Cu cell. MnO_2@Cu has a short circuit duration of 186 h, which suggests that 372 mA h cm^{-2} lithium may be plated on it (Fig. 3a). The voltage of bare Cu, in contrast, starts to quickly decline after 65 h, which may indicate a rapid cell short circuit (Fig. 2a).

The CE, analyzed as the ratio of stripping to plating capacity, is a critical measure of the viability, applicability, and cyclability of lithium deposition.[75] Fig. 2b and 3b show the findings as CE *vs.* cycle number for cells at 2 mA cm^{-2} with the same 2 mA h cm^{-2} capacity. MnO_2@Cu exhibited extended and stable cycles with a good CE of 84% up to 100 cycles, in contrast to pure Cu, which has an unstable CE and declines quickly after 35 cycles at 2 mA cm^{-2}. An increase in irreversible side reactions, such as the weak SEI layer deterioration, is linked to the quick decay of Cu.[76,77] More specifically, at 2 mA cm^{-2}, the Li//MnO_2@Cu cell displays stable CE for 186 h. Be aware that certain processes, such as quick Li^+ intercalation and Mn–Li alloying into the MnO_2 structure, may occur during the whole cycle and lower the associated CE of the MnO_2@Cu anode, particularly during the first few cycles. However, due to the development of a steady SEI and expansion of Li metal without dendrites, the CE will continue to be remarkably stable in the

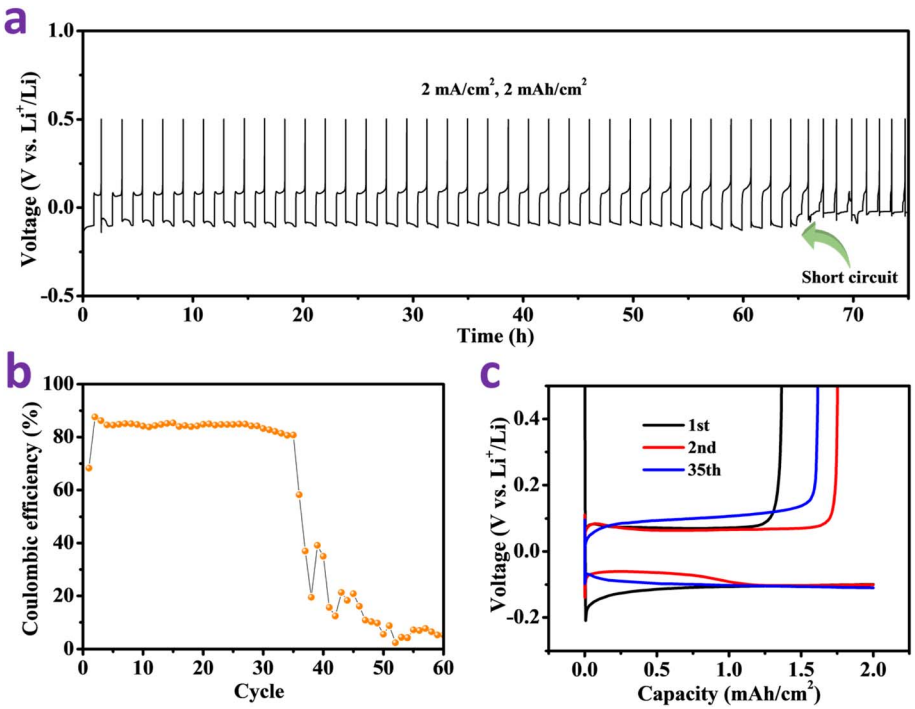

Fig. 2 (a) Cycling performance, (b) coulombic efficiency, and (c) corresponding voltage profiles of lithium plating/stripping on bare Cu at a current density of 2 mA cm^{-2} and an areal capacity of 2 mA h cm^{-2}.

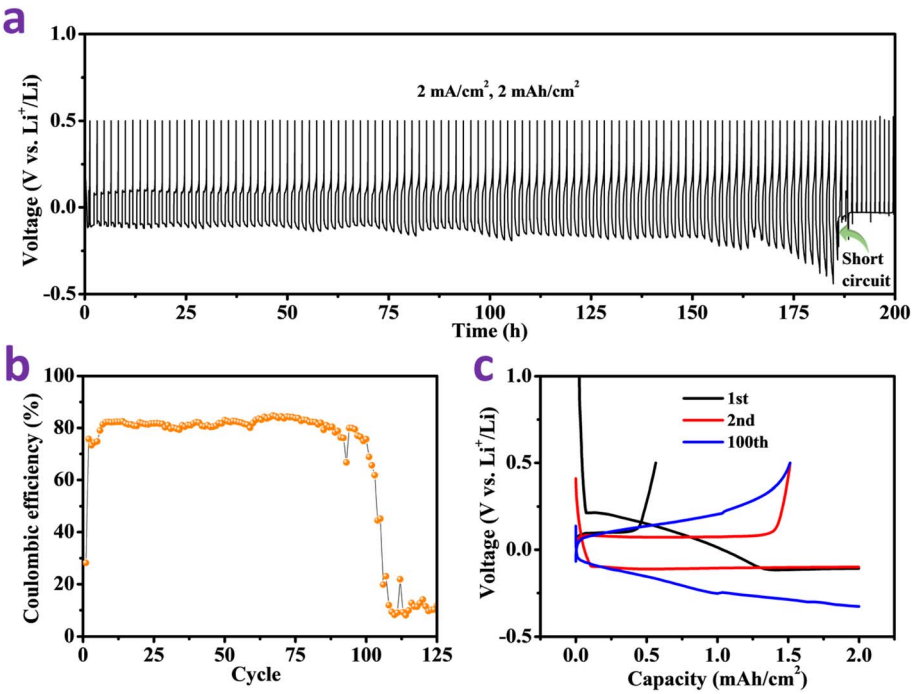

Fig. 3 (a) Cycling performance, (b) coulombic efficiency, and (c) corresponding voltage profiles of lithium plating/stripping on MnO_2@Cu at a current density 2 mA cm^{-2} and areal capacity of 2 mA h cm^{-2}.

cycles that follow. Long-term cycling performance and stable CE on modified current collectors are also explained by the plating of Li on the MnO_2 nanostructure, which remains generally stable even after 100 cycles.[78] The cyclic performance of the Li// Cu cell, however, is much shorter, lasting fewer than 65 h and 35 cycles, respectively.

Fig. 2c and 3c show the plating/stripping profiles of Cu and MnO_2@Cu, respectively. The change in the sharp voltage tip and following steady voltage was compared in order to calculate the nucleation overpotential of lithium plating on bare Cu and MnO_2@Cu current collectors.[79,80] A lower polarization value for the Li//MnO_2@Cu cell utilizing the MnO_2@Cu electrode than the bare Cu electrode suggests the low Li^+ and e− transportation resistance in the MnO_2@Cu electrode during operation.[81,82] The improved lithiophilic properties of the MnO_2@Cu electrode are shown by the fact that its initial nucleation overpotential is lower than that of the bare Cu substrate.[83,84] The lithiophilic coating, which also makes it easier for uniform Li deposition and increases the reversibility of lithium plating/ stripping cycles, is what causes the lower Li nucleation overpotential on MnO_2@Cu in comparison to the Cu host.[85] The nucleation overpotential, which temporarily emerges during the early phases of Li deposition, is a reflection of the electrode surface's lithiophilicity.[86] It varies from the mass-transfer overpotential, which is governed by Li^+ ion mobility and current density and lasts throughout deposition. The nucleation overpotential is illustrated by the rapid voltage decrease in the first cycle, as shown in Fig. 3c.[81,82] After a few cycles, the potential of lithium plating and stripping varies according to the number of cycles performed. They don't change for the next 35 h of testing. As the nucleation potential increases during this process, the areal energy for nucleation decreases.[87]

In Fig. 4, the sequential deposition of Li on MnO_2@Cu is conceptually shown. Metallic Li is used to cover the MnO_2 nanorods with a smooth layer of Li, and further Li deposition fills in the spaces between the nanorods to create a homogeneous Li metal anode free of Li dendrites. The deposited MnO_2 thin film on the Cu current collector reacts with lithium in the first cycle before the metallic lithium phase is formed, hindering the formation of Li dendrites, according to a very insignificant nucleation overpotential value. At normal temperature, bare Cu has little to no solubility in lithium metal, which causes a substantial nucleation overpotential.[88]

Fig. 5a and 6a show the voltage profiles of lithium plating/ stripping in the case of two electrodes at various current densities (2–5 mA cm^{-2}) and capacities (2–5 mA h cm^{-2}). MnO_2@Cu exhibits a stable discharge plateau between 2 and 5 mA cm^{-2} (Fig. 6a), but short-circuiting instigated by Li dendrites causes bare Cu's discharge plateau at 3 mA cm^{-2} to fluctuate (Fig. 5a). Actually, when the capacity increases from 2 to 5 mA h cm^{-2}, the Li dendrites formation accelerates in the half-cells with bare Cu electrodes. The MnO_2@Cu electrode nonetheless exhibits a consistent cycling reversibility under challenging testing conditions (plating capacity of 5 mA h cm^{-2}). The electrode sustains 20 cycles even when a higher current density is used. However, due to irregular lithium nucleation and dendrite growth, the bare Cu collector exhibits significant fluctuations and short circuits as well.

Fig. 5b and 6b show the CE of lithium plating/stripping cycles associated with Cu and MnO_2@Cu at different areal capacities and current densities. However, the CE of the Cu

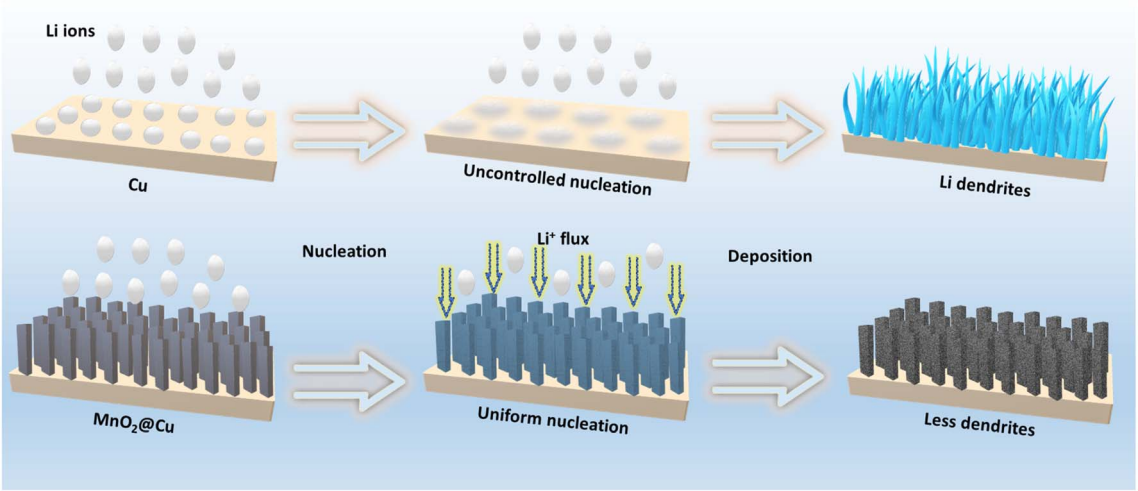

Fig. 4 Lithium growth behavior during plating on bare Cu and MnO_2-modified Cu current collectors.

anode fluctuates randomly at the relatively higher areal capacity of 5 mA h cm^{-2}, and the corresponding battery fails at the end of its cycling. All of the MnO_2@Cu collectors show better CE values and cycling capabilities that last longer and are more stable at varying current densities. The MnO_2@Cu anode's CE is capable of supporting Li areal capacities of 2 to 5 mA h cm^{-2}. Bare Cu collectors could only cycle for a maximum of 20 cycles, whereas MnO_2@C collectors could cycle for more than 20 cycles with high CE. It is noteworthy that the CE in our experiment exhibits stability despite a high current density and a high deposition capacity, indicating the exceptional electrochemical qualities of the MnO_2@Cu collector. This results from the MnO_2@Cu collector's favorable lithiophilic properties, which reduce the associated nucleation overpotential, lower the related deposition barrier, and constrain lithium dendrite growth throughout plating/stripping cycles. The MnO_2@Cu current collectors, in contrast, also demonstrated clear benefits compared to Cu collectors. For bare Cu electrodes, a short circuit occurs at the fifth cycle.

The voltage profiles of the Cu and MnO_2@Cu anodes are shown in Fig. 5c and 6c, respectively. MnO_2@Cu's discharge profiles are stable during cycling. According to the outcomes of

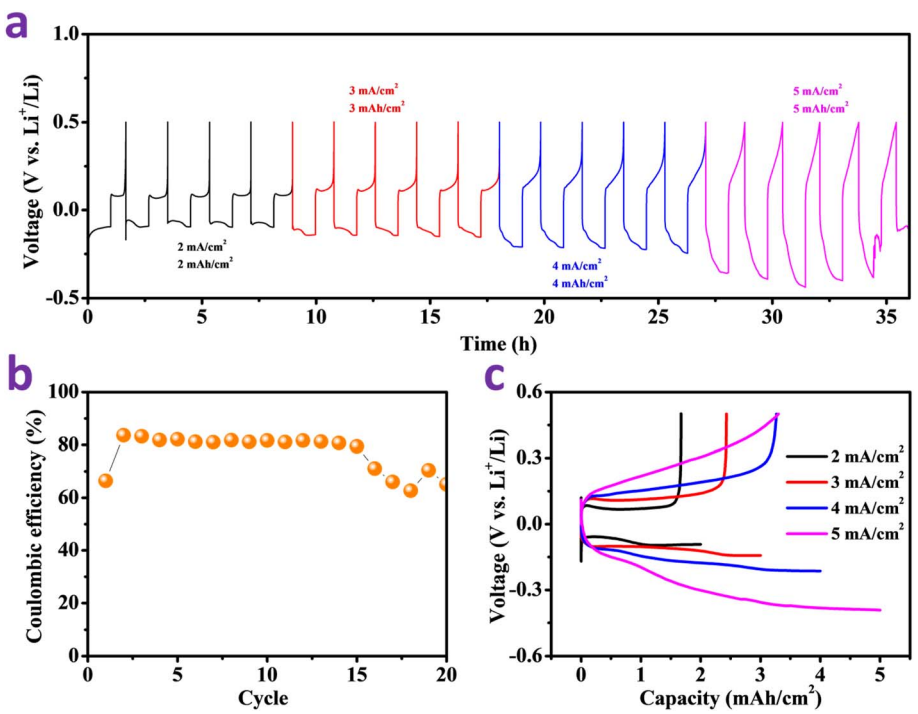

Fig. 5 (a) Rate performance, (b) coulombic efficiency, and (c) corresponding voltage profiles of lithium plating/stripping on bare Cu at current densities of 2–5 mA cm^{-2} and areal capacities of 2–5 mA h cm^{-2}.

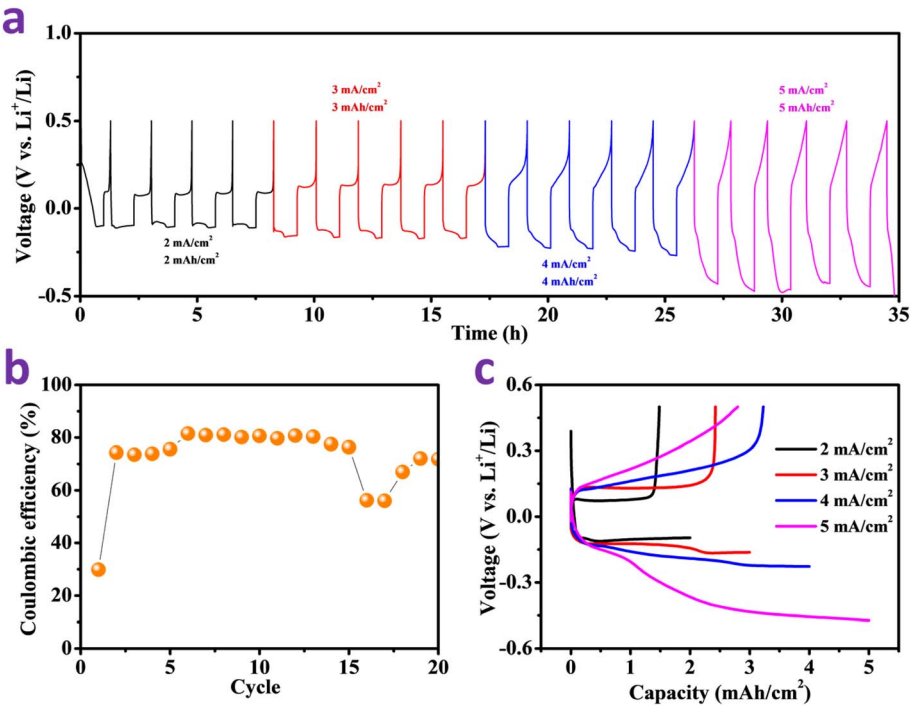

Fig. 6 (a) Rate performance, (b) coulombic efficiency, and (c) corresponding voltage profiles of lithium plating/stripping on MnO_2@Cu at current densities of 2–5 mA cm^{-2} and areal capacities of 2–5 mA h cm^{-2}.

CE profiles, the stripping areal capacity of MnO_2@Cu exhibits improved coincidence and doesn't visibly decline as the cycle number increases. The inability of the Cu electrodes to discharge at 5 mA cm^{-2} current density may be attributed to the rapid formation of lithium dendrites. Due to the large surface area of the MnO_2 nanorods and their lithiophilic coating, MnO_2@Cu has a low Li overpotential, as shown in Fig. 6c. The detailed rate performances (2–7 mA cm^{-2}) have been added to the ESI (Fig. S2).†

It is obvious that the lithium plating/stripping properties of copper foil and MnO_2@Cu are different. Since copper foil has a lower nucleation potential than MnO_2@Cu, a large amount of nucleation capacity is needed before lithium can be plated on MnO_2@Cu. These disparities are thought to be caused by variations in the surface characteristics of these two current collectors. Due to MnO_2's porous structure, lithium may be easily plated on it, which results in the development of condensed lithium on its surface. Given that MnO_2@Cu has a much stronger chemical affinity for metallic lithium, this may result in a lower nucleation overpotential for MnO_2@Cu. In contrast, when using Cu foil, the solvated lithium ions inevitably plate and undergo exfoliation or pulverization. It is clear from the discussion above that the MnO_2 nanorods on Cu current collectors made it easier to form an excellent SEI layer, homogenize ion flux scattering, improve Li^+ conductivity, allow for uniform lithium deposition, and prevent lithium dendrite growth, which together enable the enhancement of plating/stripping performance. Table S1† compares the performance of lithium-ion batteries associated with various Cu-modified current collectors.

4. Conclusions

Here, we offer a straightforward, scalable technique for modifying the Cu collector using MnO_2 nanorods. Strong lithiophilicity of MnO_2 nanorods may influence the process of the lithium plating and prevent growth of Li dendrites, in addition to lowering the nucleation barrier by acting as nuclei to direct homogeneous lithium nucleation. MnO_2 may provide a large number of active sites to promote Li nucleation. Strong ionic conductivity on the MnO_2 protective layer and high electron conductivity inside nanorods may be used to coordinate the control of Li^+ flux and electron distribution, leading to dendrite-free Li plating/stripping behavior. Additionally, the lithium metal stored in the space between nanorods can effectively reduce volume change during repeated charging and discharging. These benefits are made possible by MnO_2 modified Cu current collectors, which also provide low overpotential and high CE. These advantages result in a simple, scalable process for manufacturing lithium metal anodes for industrial use, which in turn promotes the fabrication of safe Li-metal batteries.

Data availability

Data are available upon request from the authors.

Conflicts of interest

There are no conflicts to declare.

Acknowledgements

Bidhan Pandit acknowledges the Iberdrola Foundation under the Marie Skłodowska-Curie Grant Agreement No. 101034297. CH acknowledges funding from the ERC Starting Grant (UKRI Guarantee fund EP/Y009908/1), the Faraday Institution research programme grants FIRG060, FIRG082, and FIRG066, and Imperial College London UKRI Impact Acceleration Account EP/X52556X/1.

References

1 A. Dutta, S. Mitra, M. Basak and T. Banerjee, *Energy Storage*, 2023, **5**, e339.
2 G. Sadeghi, *Energy Storage Mater.*, 2022, **46**, 192–222.
3 B. Pandit, M. T. Sougrati, B. Fraisse and L. Monconduit, *Nano Energy*, 2022, **95**, 107010.
4 X. Zhao, Z. Zhao-Karger, M. Fichtner and X. Shen, *Angew. Chem., Int. Ed.*, 2020, **59**, 5902–5949.
5 M. Abdel-Monem, O. Hegazy, N. Omar, K. Trad, P. Van den Bossche and J. Van Mierlo, in *2017 19th European Conference on Power Electronics and Applications (EPE'17 ECCE Europe)*, IEEE, 2017, vol. 2017-Janua, p. P.1-P.16.
6 M. A. Jamil, G. Ali, K. I. Khan, F. Jan Iftikhar, S. Zaman, S. F. Shaikh, B. Pandit, Q. Wali and S. A. Patil, *J. Alloys Compd.*, 2022, **900**, 163447.
7 J. M. Naranjo-Balseca, C. S. Martínez-Cisneros, B. Pandit, B. Levenfeld, J.-Y. Sanchez and A. Varez, *J. Power Sources*, 2025, **630**, 236175.
8 Y. Tian, G. Zeng, A. Rutt, T. Shi, H. Kim, J. Wang, J. Koettgen, Y. Sun, B. Ouyang, T. Chen, Z. Lun, Z. Rong, K. Persson and G. Ceder, *Chem. Rev.*, 2021, **121**, 1623–1669.
9 J. W. Choi and D. Aurbach, *Nat. Rev. Mater.*, 2016, **1**, 16013.
10 V. Ahuja, S. Singh, R. Vengarathody and P. Senguttuvan, *ECS Meet. Abstr.*, 2021, MA2021-01, pp. 254.
11 Y. Fan, H. Li, X. He, Y. Huang, C. Sun, T. Zhu, H. Liu, E. Huangzhang, F. Sun and J. Nan, *ACS Appl. Energy Mater.*, 2022, **5**, 10034–10044.
12 Y. Fan, H. Li, X. He, Y. Huang, C. Sun, T. Zhu, H. Liu, E. Huangzhang, F. Sun and J. Nan, *ACS Appl. Energy Mater.*, 2022, **5**, 10034–10044.
13 H. Zhang, R. Li, L. Chen, Y. Fan, H. Zhang, R. Zhang, L. Zheng, J. Zhang, S. Ding, Y. Wu, B. Ma, S. Zhang, T. Deng, L. Chen, Y. Shen and X. Fan, *Angew. Chem.*, 2023, **135**, e202218970.
14 W. Jiang, S. Wang, Y. Wang, J. Hu, D. Yang and W. Zhang, *Energy Technol.*, 2023, 2300053.
15 R. Li, Y. Fan, C. Zhao, A. Hu, B. Zhou, M. He, J. Chen, Z. Yan, Y. Pan and J. Long, *Small Methods*, 2022, 2201177.
16 S. Yuan, K. Ding, X. Zeng, D. Bin, Y. Zhang, P. Dong and Y. Wang, *Adv. Mater.*, 2023, **35**, 2206228.
17 D. Yan, H. Y. Yang and Y. Bai, *Nano Res.*, 2023, 1–18.
18 L. Zhou, D. L. Danilov, R. Eichel and P. H. L. Notten, *Adv. Energy Mater.*, 2021, **11**, 2001304.
19 Y. Gao, Q. Guo, Q. Zhang, Y. Cui and Z. Zheng, *Adv. Energy Mater.*, 2021, **11**, 2002580.
20 M. R. Al Khazraji, J. Wang and S. Wei, *Energy Technol.*, 2023, **11**, 2200944.
21 H.-F. Wang, X.-X. Wang, F. Li and J.-J. Xu, *Small Sci.*, 2022, **2**, 2200005.
22 L. Liu, H. Guo, L. Fu, S. Chou, S. Thiele, Y. Wu and J. Wang, *Small*, 2021, **17**, 1903854.
23 X. Zou, Q. Lu, K. Liao and Z. Shao, *Energy Storage Mater.*, 2022, **45**, 869–902.
24 N. Kim, H. Cha, S. Chae, T. Lee, Y. Lee, Y. Kim, J. Sung and J. Cho, *Energy Environ. Sci.*, 2023, **16**, 2505–2517.
25 B. Pandit, S. R. Rondiya, S. F. Shaikh, M. Ubaidullah, R. Amaral, N. Y. Dzade, E. S. Goda, A. ul Hassan Sarwar Rana, H. Singh Gill and T. Ahmad, *J. Colloid Interface Sci.*, 2023, **633**, 886–896.
26 Q. Liu, R. Liu, Y. Cui, M. Zhou, J. Zeng, B. Zheng, S. Liu, Y. Zhu and D. Wu, *Adv. Mater.*, 2022, **34**, 2108437.
27 J. Deng, X. Yang and G. Zhang, *Mater. Today Commun.*, 2022, **31**, 103570.
28 Z. Deng, J. Gu, Y. Li, S. Li, J. Peng, X. Li, J. Luo, Y. Huang, C. Fang, Q. Li, J. Han, Y. Huang and Y. Zhao, *Electrochim. Acta*, 2019, **298**, 121–126.
29 A. Wang, S. Kadam, H. Li, S. Shi and Y. Qi, *npj Comput. Mater.*, 2018, **4**, 15.
30 H. Wu, H. Jia, C. Wang, J. Zhang and W. Xu, *Adv. Energy Mater.*, 2021, **11**, 2003092.
31 H. Adenusi, G. A. Chass, S. Passerini, K. V Tian and G. Chen, *Adv. Energy Mater.*, 2023, **13**, 2203307.
32 Q. Li, B. Quan, W. Li, J. Lu, J. Zheng, X. Yu, J. Li and H. Li, *Nano Energy*, 2018, **45**, 463–470.
33 Y. Liu, D. Lin, Z. Liang, J. Zhao, K. Yan and Y. Cui, *Nat. Commun.*, 2016, **7**, 10992.
34 Y. Sun, C. Zhao, K. R. Adair, Y. Zhao, L. V. Goncharova, J. Liang, C. Wang, J. Li, R. Li, M. Cai, T.-K. Sham and X. Sun, *Energy Environ. Sci.*, 2021, **14**, 4085–4094.
35 R. Cong, J.-Y. Choi, J.-B. Song, M. Jo, H. Lee and C.-S. Lee, *Sci. Rep.*, 2021, **11**, 1283.
36 X. Zhang, A. Wang, X. Liu and J. Luo, *Acc. Chem. Res.*, 2019, **52**, 3223–3232.
37 H. Liu, X. B. Cheng, Z. Jin, R. Zhang, G. Wang, L. Q. Chen, Q. B. Liu, J. Q. Huang and Q. Zhang, *EnergyChem*, 2019, **1**, 100003.
38 H. Liu, X.-B. Cheng, Z. Jin, R. Zhang, G. Wang, L.-Q. Chen, Q.-B. Liu, J.-Q. Huang and Q. Zhang, *EnergyChem*, 2019, **1**, 100003.
39 H. Liu, X. Chen, X. Cheng, B. Li, R. Zhang, B. Wang, X. Chen and Q. Zhang, *Small Methods*, 2019, **3**, 1800354.
40 J. Meng, F. Chu, J. Hu and C. Li, *Adv. Funct. Mater.*, 2019, **29**, 1902220.
41 X. Guan, A. Wang, S. Liu, G. Li, F. Liang, Y.-W. Yang, X. Liu and J. Luo, *Small*, 2018, **14**, 1801423.
42 Y. Zhu, J. Xie, A. Pei, B. Liu, Y. Wu, D. Lin, J. Li, H. Wang, H. Chen, J. Xu, A. Yang, C.-L. Wu, H. Wang, W. Chen and Y. Cui, *Nat. Commun.*, 2019, **10**, 2067.
43 T. Chen, W. Kong, P. Zhao, H. Lin, Y. Hu, R. Chen, W. Yan and Z. Jin, *Chem. Mater.*, 2019, **31**, 7565–7573.
44 B. Li, Y. Wang and S. Yang, *Adv. Energy Mater.*, 2018, **8**, 1702296.

45 G. Wang, H. Wang, B. Zhong, L. Zhang and J. Zhang, in *Electrochemical Energy*, ed. J. Z. Pei Kang Shen, C.-Y. Wang, S. P. Jiang and X. Sun, CRC Press, Boca Raton, 1st edn, 2015, pp. 479–492.
46 H. Zhang, G. G. Eshetu, X. Judez, C. Li, L. M. Rodriguez-Martínez and M. Armand, *Angew. Chem., Int. Ed.*, 2018, **57**, 15002–15027.
47 L. Li, H. Dai and C. Wang, *Nano Sel.*, 2021, **2**, 16–36.
48 S. Li, Z. Luo, L. Li, J. Hu, G. Zou, H. Hou and X. Ji, *Energy Storage Mater.*, 2020, **32**, 306–319.
49 D. Kang, M. Xiao and J. P. Lemmon, *Batteries Supercaps*, 2021, **4**, 445–455.
50 U. S. Meda, L. Lal, S. M and P. Garg, *J. Energy Storage*, 2022, **47**, 103564.
51 H. Wang and Y. Tang, *Chem. Res. Chin. Univ.*, 2020, **36**, 402–409.
52 S. Ni, S. Tan, Q. An and L. Mai, *J. Energy Chem.*, 2020, **44**, 73–89.
53 D. Li, B. Chen, H. Hu and W. Lai, *Adv. Sustainable Syst.*, 2022, **6**, 2200010.
54 T. Wei, J. Lu, M. Wang, C. Sun, Q. Zhang, S. Wang, Y. Zhou, D. Chen and Y.-Q. Lan, *Chin. J. Chem.*, 2023, **41**, 1861–1874.
55 C. S. Martinez-Cisneros, B. Pandit, B. Levenfeld, A. Varez and J.-Y. Sanchez, *J. Power Sources*, 2023, **559**, 232644.
56 C. S. Martínez-Cisneros, B. Pandit, C. Antonelli, J. Y. Sanchez, B. Levenfeld and A. Varez, *J. Eur. Ceram. Soc.*, 2021, **41**, 7723–7733.
57 J. M. Naranjo-Balseca, C. S. Martínez-Cisneros, B. Pandit and A. Várez, *J. Eur. Ceram. Soc.*, 2023, **43**, 4826–4836.
58 G. Wang, X. Xiong, P. Zou, X. Fu, Z. Lin, Y. Li, Y. Liu, C. Yang and M. Liu, *Chem. Eng. J.*, 2019, **378**, 122243.
59 Q. Zhang, J. Luan, Y. Tang, X. Ji, S. Wang and H. Wang, *J. Mater. Chem. A*, 2018, **6**, 18444–18448.
60 C. Zhang, W. Lv, G. Zhou, Z. Huang, Y. Zhang, R. Lyu, H. Wu, Q. Yun, F. Kang and Q.-H. Yang, *Adv. Energy Mater.*, 2018, **8**, 1703404.
61 K. Tang, H. Gao, J. Xiao, M. Long, J. Chen, H. Liu and G. Wang, *Chem. Eng. J.*, 2022, **436**, 134698.
62 M. Barghamadi, A. S. Best, A. I. Bhatt, A. F. Hollenkamp, M. Musameh, R. J. Rees and T. Rüther, *Energy Environ. Sci.*, 2014, **7**, 3902–3920.
63 L. F. Nazar, M. Cuisinier and Q. Pang, *MRS Bull.*, 2014, **39**, 436–442.
64 A. Rosenman, E. Markevich, G. Salitra, D. Aurbach, A. Garsuch and F. F. Chesneau, *Adv. Energy Mater.*, 2015, **5**, 1500212.
65 S. S. Zhang, *Electrochim. Acta*, 2013, **97**, 226–230.
66 S. Xiong, K. Xie, Y. Diao and X. Hong, *Electrochim. Acta*, 2012, **83**, 78–86.
67 S. Xiong, K. Xie, Y. Diao and X. Hong, *J. Power Sources*, 2014, **246**, 840–845.
68 B. Pandit, E. S. Goda, M. H. Abu Elella, A. ur Rehman, S. Eun Hong, S. R. Rondiya, P. Barkataki, S. F. Shaikh, A. M. Al-Enizi, S. M. El-Bahy and K. Ro Yoon, *J. Energy Chem.*, 2022, **65**, 116–126.
69 B. Pandit, M. Johansen, C. Susana Martínez-Cisneros, J. M. Naranjo-Balseca, B. Levenfeld, D. B. Ravnsbæk and A. Varez, *Chem. Mater.*, 2024, **36**, 2314–2324.
70 S. F. Shaikh, S. Aftab, B. Pandit, A. M. Al-Enizi, M. Ubaidullah, S. Ekar, S. Hussain, Y. B. Khollam, P. S. More and R. S. Mane, *Dalton Trans.*, 2023, **52**, 11481–11488.
71 B. Pandit, M. Johansen, B. P. Andersen, C. S. Martínez-Cisneros, B. Levenfeld, D. B. Ravnsbæk and A. Varez, *Chem. Eng. J.*, 2023, **472**, 144509.
72 B. Pandit, B. Fraisse, L. Stievano, L. Monconduit and M. T. Sougrati, *Electrochim. Acta*, 2022, **409**, 139997.
73 B. Pandit, S. R. Rondiya, N. Y. Dzade, S. F. Shaikh, N. Kumar, E. S. Goda, A. A. Al-Kahtani, R. S. Mane, S. Mathur and R. R. Salunkhe, *ACS Appl. Mater. Interfaces*, 2021, **13**, 11433–11441.
74 Z.-H. Huang, Y. Song, D.-Y. Feng, Z. Sun, X. Sun and X.-X. Liu, *ACS Nano*, 2018, **12**, 3557–3567.
75 L. Liu, Y.-X. Yin, J.-Y. Li, N.-W. Li, X.-X. Zeng, H. Ye, Y.-G. Guo and L.-J. Wan, *Joule*, 2017, **1**, 563–575.
76 R. Pathak, K. Chen, A. Gurung, K. M. Reza, B. Bahrami, J. Pokharel, A. Baniya, W. He, F. Wu, Y. Zhou, K. Xu and Q. Qiao, *Nat. Commun.*, 2020, **11**, 93.
77 P. Xu, X. Hu, X. Liu, X. Lin, X. Fan, X. Cui, C. Sun, Q. Wu, X. Lian, R. Yuan, M. Zheng and Q. Dong, *Energy Storage Mater.*, 2021, **38**, 190–199.
78 S. Cui, P. Zhai, W. Yang, Y. Wei, J. Xiao, L. Deng and Y. Gong, *Small*, 2020, **16**, 1905620.
79 Z. Zhang, J. Wang, X. Yan, S. Zhang, W. Yang, Z. Zhuang and W.-Q. Han, *Energy Storage Mater.*, 2020, **29**, 332–340.
80 C. Wei, H. Fei, Y. An, Y. Tao, J. Feng and Y. Qian, *J. Mater. Chem. A*, 2019, **7**, 18861–18870.
81 S. Chen, K. Tao, X. Chen, Y. Meng, M. Wang, J. Zhou, C. Chen, Y. Wang, K. Nam Hui, C. W. Bielawski and J. Geng, *Chem. - Eur. J.*, 2021, **27**, 15706–15715.
82 S.-S. Chi, Y. Liu, W.-L. Song, L.-Z. Fan and Q. Zhang, *Adv. Funct. Mater.*, 2017, **27**, 1700348.
83 S. Wang, Y. Wang, Y. Song, J. Zhang, X. Jia, J. Yang, D. Shao, Y. Li, J. Liao and H. Song, *Energy Storage Mater.*, 2022, **50**, 505–513.
84 Y. Sun, J. Zhou, H. Ji, J. Liu, T. Qian and C. Yan, *ACS Appl. Mater. Interfaces*, 2019, **11**, 32008–32014.
85 M. Baek, J. Kim, K. Jeong, S. Yang, H. Kim, J. Lee, M. Kim, K. J. Kim and J. W. Choi, *Nat. Commun.*, 2023, **14**, 1296.
86 Y. Sun, J. Zhou, H. Ji, J. Liu, T. Qian and C. Yan, *ACS Appl. Mater. Interfaces*, 2019, **11**, 32008–32014.
87 G. Yang, Y. Li, Y. Tong, J. Qiu, S. Liu, S. Zhang, Z. Guan, B. Xu, Z. Wang and L. Chen, *Nano Lett.*, 2019, **19**, 494–499.
88 C. Yang, Y. Yao, S. He, H. Xie, E. Hitz and L. Hu, *Adv. Mater.*, 2017, **29**, 1702714.